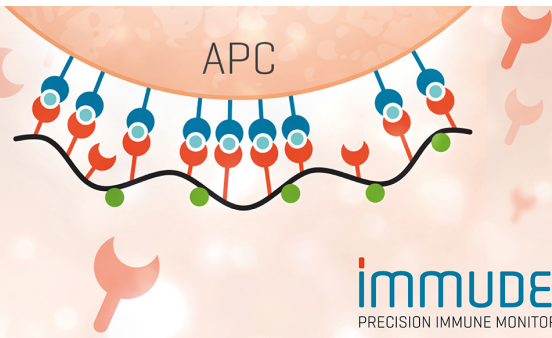


TCR Solutions Detect Antigen Presentation

- Immunex produces your TCRs
- Soluble TCRs and TCR Dextramer®



IMMUDEx[®]
PRECISION IMMUNE MONITORING

The Journal of Immunology

RESEARCH ARTICLE | JULY 05 2023

The Polyanionic Drug Suramin Neutralizes Histones and Prevents Endotheliopathy ✓

Nuria Villalba; ... et. al

J Immunol (2023) 211 (4): 648–657.

<https://doi.org/10.4049/jimmunol.2200703>

Related Content

Inhibition of lipopolysaccharide and IL-1 but not of TNF-induced activation of human endothelial cells by suramin.

J Immunol (September,1994)

Top Reads

J Immunol (August,2023)

Suramin inhibits the stimulation of acute phase plasma protein genes by IL-6-type cytokines in rat hepatoma cells.

J Immunol (August,1993)

The Polymeric Drug Suramin Neutralizes Histones and Prevents Endotheliopathy

Nuria Villalba,^{*,1} Adrian M. Sackheim,^{*} Michael A. Lawson,^{*,2} Laurel Haines,^{*,3} Yen-Lin Chen,[†] Swapnil K. Sonkusare,[†] Yong-Tao Ma,[‡] Jianing Li,[‡] Devdoot Majumdar,^{§,¶} Beth A. Bouchard,^{||,4} Jonathan E. Boyson,[¶] Matthew E. Poynter,[#] Mark T. Nelson,^{**,‡} and Kalev Freeman^{*,**}

Drugs are needed to protect against the neutrophil-derived histones responsible for endothelial injury in acute inflammatory conditions such as trauma and sepsis. Heparin and other polyanions can neutralize histones but challenges with dosing or side effects such as bleeding limit clinical application. In this study, we demonstrate that suramin, a widely available polyanionic drug, completely neutralizes the toxic effects of individual histones, but not citrullinated histones from neutrophil extracellular traps. The sulfate groups on suramin form stable electrostatic interactions with hydrogen bonds in the histone octamer with a dissociation constant of 250 nM. In cultured endothelial cells (Ea.Hy926), histone-induced thrombin generation was significantly decreased by suramin. In isolated murine blood vessels, suramin abolished aberrant endothelial cell calcium signals and rescued impaired endothelial-dependent vasodilation caused by histones. Suramin significantly decreased pulmonary endothelial cell ICAM-1 expression and neutrophil recruitment caused by infusion of sublethal doses of histones in vivo. Suramin also prevented histone-induced lung endothelial cell cytotoxicity in vitro and lung edema, intra-alveolar hemorrhage, and mortality in mice receiving a lethal dose of histones. Protection of vascular endothelial function from histone-induced damage is a novel mechanism of action for suramin with therapeutic implications for conditions characterized by elevated histone levels. *The Journal of Immunology*, 2023, 211: 648–657.

Acute endotheliopathy is a clinical syndrome resulting from extensive tissue injury in trauma and sepsis, including that attributable to SARS-CoV-2 infection. Endotheliopathy is characterized by widespread disruption of endothelial-dependent vasodilatory function, barrier integrity, and hemostasis, which all contribute to thromboinflammation, organ failure, and mortality (1, 2). Extracellular histones are major mediators of endotheliopathy, as shown by the efficacy of antihistone Abs in preventing systemic inflammation and mortality in animal models of sepsis and endotoxemia through LPS infusion (3, 4). Histones enter the circulation when released by cellular apoptosis or necrosis (5–7), and in innate immunity, when activation of neutrophils leads to the release of chromatin in the form of neutrophil extracellular traps (NETs). These NETs contain granular enzymes and peptides that aid in clearing bacteria,

as well as nuclear proteins, predominantly histones (3, 4). Nucleosomes induce cytokine production at low concentrations, but high concentrations kill cells (8). Evidence of NET-induced endothelial damage has been reported in COVID-19 (9), atherosclerosis (10, 11), ischemia/reperfusion (12), and venous thrombosis (13, 14). Plasma nucleases act on DNA/histone complexes circulating in the blood to degrade the nucleic acids, exposing the highly cationic histones that function as damage-associated molecular pattern proteins, activating the immune system and causing additional toxicity (15–17). Free histones are found at low levels (2–5 µg/ml) in the circulation in uninjured humans, but levels can reach 20–100 µg/ml in COVID-19 patients (18) and up to 250 µg/ml in the acute period following severe trauma before they are degraded over hours and days by the protease-activated protein C (19). At high concentrations, histones

^{*}Department of Emergency Medicine, University of Vermont, Burlington, VT; [†]Department of Molecular Physiology and Biological Physics, University of Virginia, Charlottesville, VA; [‡]Department of Chemistry, University of Vermont, Burlington, VT; [§]Department of Microbiology and Molecular Genetics, University of Vermont, Burlington, VT; [¶]Department of Surgery, University of Vermont, Burlington, VT; ^{||}Department of Biochemistry, University of Vermont, Burlington, VT; [#]Department of Medicine, University of Vermont, Burlington, VT; ^{**}Department of Pharmacology, University of Vermont, Burlington, VT; and [‡]Division of Cardiovascular Sciences, University of Manchester, Manchester, United Kingdom

¹Current address: Department of Molecular Pharmacology and Physiology, University of South Florida, Tampa, FL.

²Current address: Department of Emergency Medicine, University of Wisconsin, Madison, WI.

³Current address: Department of Microbiology, Immunology, and Pathology, Colorado State University, Fort Collins, CO.

⁴Current address: Prolytix, Essex Junction, VT.

ORCIDs: 0000-0001-5903-2937 (N.V.); 0000-0001-8443-943X (M.A.L.); 0000-0002-8410-248X (L.H.); 0000-0001-9587-9342 (S.K.S.); 0000-0002-0399-566X (B.A.B.); 0000-0002-7578-4570 (M.E.P.); 0000-0002-6608-8784 (M.T.N.); 0000-0003-4817-2955 (K.F.).

Received for publication September 19, 2022. Accepted for publication June 9, 2023.

This work was supported by the Totman Medical Research Trust (to M.T.N.), HORIZON EUROPE Framework Programme Grant 666881 (SVDs@target, to M.T.N.), as well as by National Institute of Neurological Disorders and Stroke Grant R01-NS-110656 (to M.T.N.),

National Institute of General Medical Sciences Grant P20-GM-135007 (to M.T.N.) and R35-GM-144099-01 (to K.F.), and National Heart, Lung, and Blood Institute Grants R01-HL-146914 (to S.K.S.), R01-HL-157407 (to S.K.S.), R01-HL-142081 (to M.E.P.), R01-HL-133920 (to M.E.P.), R35-HL-140027 (to M.T.N.), and 1OT2HL156812 (to K.F.); U.S. Department of Defense/The Henry M. Jackson Foundation for the Advancement of Military Medicine Grant HU001-18-2-0016 (to K.F.); NIH Office of the Director Grant S10-OD-026843 (to J.E.B.); National Institute of Allergy and Infectious Diseases Grant R03-AI153902 (to J.E.B.); and by American Chemical Society Grant ACS-PRF-58219-DNI (to J.L. and Y.-T.M.). Imaging work was performed at the Microscopy Imaging Center at the University of Vermont (RRID SCR_018821). The views and conclusions contained in this document are those of the authors and should not be interpreted as representing the official policies, either expressed or implied, of the National Institutes of Health.

N.V., A.M.S., S.K.S., J.L., B.A.B., J.E.B., M.E.P., M.T.N., and K.F. designed research; N.V., A.M.S., M.A.L., L.H., Y.-L.C., S.K.S., and Y.-T.M. performed research; N.V., A.M.S., M.A.L., S.K.S., J.L., D.M., B.A.B., J.E.B., M.E.P., M.T.N., and K.F. analyzed data; and N.V., A.M.S., and K.F. drafted the paper. All authors contributed to edits and revisions of the final manuscript.

Address correspondence and reprint requests to Dr. Kalev Freeman, University of Vermont, 149 Beaumont Avenue, Firestone Medical Research Building 452, Burlington, VT 05405. E-mail address: kalev.freeman@med.uvm.edu

The online version of this article contains supplemental material.

Abbreviations used in this article: BALF, bronchoalveolar lavage fluid; CI, confidence interval; NET, neutrophil extracellular trap; PI, propidium iodide; TF, tissue factor.

Copyright © 2023 by The American Association of Immunologists, Inc. 0022-1767/23/\$37.50

can activate platelets and damage vascular cells, particularly pulmonary (19) and mesenteric endothelial cells (20), vascular smooth muscle cells (11), and erythrocytes (21, 22), but histones are not directly toxic to endothelial cells in the cerebral vasculature (23). Histones activate and injure endothelial cells through mechanisms including calcium overload (3, 20), pyroptosis through NLRP3 inflammasome and TLR activation (6, 24–27), and disassembly of adherens junctions causing loss of barrier function (23, 28). Histones, similar to other cations, can also bind directly to anionic membrane phospholipids in stoichiometric ratios (29, 30), with high concentrations leading to disruption of lipid bilayers (11, 31). Furthermore, histones deposited on the lumen of blood vessels can also attract monocytes in a surface charge-dependent fashion, causing atherosclerosis (4). Elevated histone levels have been linked to widespread endothelial injury and organ damage in human patients after trauma (19, 32–38) and other conditions including ischemic stroke (39), sepsis (3), pancreatitis (40), and acute respiratory distress syndrome (41, 42).

The critical unmet need for therapeutics that protect the vascular endothelium from histone-mediated injury has become of immediate relevance in the context of the SARS-CoV-2 pandemic (1, 9, 43). It was recently demonstrated that the polyanionic agent defibrotide can neutralize the pathological effects of extracellular histones (44). This is important, because it suggests a strategy to protect blood vessels from the products of NETosis. However, defibrotide is an expensive drug that typically requires dosing every 6 h. Other synthetic polyanions can also block histone-induced toxicity (22), but these have not yet been Food and Drug Administration approved for human use. We hypothesized that suramin, a polyanionic drug that is also safe, inexpensive, and widely available, would effectively prevent histone-induced endotheliopathy. First synthesized by Bayer in 1917 as part of a drug discovery program for trypanosomiasis (African sleeping sickness), suramin is a bis-polysulfonated naphthylurea hexaanion with activity against trypanosomes in both animal models and humans (45). Suramin has been used clinically for >100 y and, importantly, is considered among the safest and most effective drugs for health care by the World Health Organization. Unlike heparan sulfate or heparin synthetic polyanions, which also bind histones, suramin dosing is infrequent (usually once per week), well tolerated, and does not cause complications associated with anticoagulation.

The objective of this study was to test the hypothesis that suramin can protect against histone-induced endothelial dysfunction. We found that suramin binds individual histones in solution, but not citrullinated histones released from NETs, which is consistent with the lack of protection against citrullinated histone-induced cytotoxicity. Histones activated cultured human endothelial cells to promote rapid thrombin generation; we found that this reaction is abolished by suramin. In pressurized murine vascular preparations, we directly tested the efficacy of suramin for preventing histone-induced aberrant endothelial calcium signaling and vasodilatory dysfunction. In a histone infusion model, we measured the extent to which suramin prevented histone-induced lung injury, endothelial cell activation, adhesion molecule expression, and pulmonary barrier disruption. Importantly, we also found that suramin completely protects against lethal doses of histones. Thus, histone binding is a novel mechanism of action for suramin, and these experiments provide support for the use of suramin as a strategy to protect against histone-induced endotheliopathy.

Materials and Methods

Animals

Male C57BL/6J mice (12 wk old; ~30 g) were purchased from The Jackson Laboratory (Bar Harbor, ME). All animals were maintained on a 12-h light/12-h dark cycle and standard diet and water ad libitum in an American

Association of Laboratory Animal Care–accredited facility. All animal experiments were approved by the University of Vermont's Institutional Animal Care and Use Committee (no. 2020-000-175), in accordance with the recommendations in the *Guide for the Care and Use of Laboratory Animals* of the National Institutes of Health, and efforts were made to minimize suffering.

In vivo histone exposure

Mice were anesthetized with 2.5% isoflurane and administered purified histones (Roche distributed by SigmaMillipore, no. 10223565001) or sterile saline (control group) as a single dose via retro-orbital sinus. Histones were diluted in sterile saline to yield doses of either 45 or 75 mg/kg.

Suramin trial in vivo

We conducted a preclinical randomized trial to establish efficacy of suramin in histone exposure. Based on the recommended initial dose of suramin (1 g for adults and 10–15 mg/kg for children) (<http://home.intekom.com/pharm/bayer/suramin.html>), we used 20 mg/kg as the human reference dose. We planned to compare $n = 10$ animals each in control (histone alone) and suramin (20 mg/kg) groups based on sample size estimations for survival analysis in a two-arm trial. For dose finding, we also included an additional arm with a higher dose of suramin ($n = 6$, 50 mg/kg). The fourth arm of the study was a control group that did not receive histones or suramin to establish the baseline ($n = 6$). Mice were randomly assigned to the four treatment groups. Suramin (AdipoGen, no. AG-CR1-3575) was administered i.p. (20 or 50 mg/kg) 1 h prior to histone infusion in the suramin groups. Animals were then anesthetized to receive either histones or controls. The primary outcome was the effect of suramin on survival in the face of a lethal dose of histones (75 mg/kg; i.v.) (1). Survival rates were determined every 5 min for 1 h.

Secondary outcomes of inflammatory biomarkers, that is, lung inflammation (histology of lavage fluid and parenchyma), pulmonary endothelial cell activation, and pulmonary vascular permeability, were studied to provide additional insight into suramin's mechanism of action in vivo. These outcomes were assessed in additional experiments utilizing a survivable dose of histones (45 mg/kg; i.v.) in mice, randomized to receive either no treatment (histones alone) or suramin (50 mg/kg). Additional controls were included that did not receive histones or suramin to establish the baseline for each outcome. All mice were terminally anesthetized and euthanized 24 h after treatment.

To assess for markers of inflammation relevant to activated endothelium, blood was collected via cardiac puncture in BD Microtainer blood collection tubes (BD Biosciences). Sera was obtained by centrifugation (1300 × g, 10 min) and frozen. Thawed sera were diluted 2-fold and cardiovascular markers were measured using a Milliplex mouse cardiovascular disease magnetic bead panel (MilliporeSigma, no. MCV1MAG-77K). Data were acquired using the Bio-Plex suspension array system and Bio-Plex Manager software.

To assess inflammation in the lung, bronchoalveolar lavage fluid (BALF) was collected and analyzed for the total number of leukocytes and total protein. Euthanized mice were tracheotomized with an 18G cannula and lavaged with 1 ml of Dulbecco's PBS (Life Technologies, Carlsbad, CA). Lavage fluid was centrifuged (1300 × g, 10 min) and cell-free supernatants were snap-frozen for total protein analysis using the Pierce bicinchoninic acid protein assay kit (Thermo Scientific, no. 23227). The pellet was resuspended with 400 μ l of PBS and total leukocyte count was measured via a hemocytometer (Neubauer chamber).

Intact lungs were also assessed for histological changes. Lungs were inflation-fixed at 20 cm H₂O pressure with buffered formalin for 24 h, embedded in paraffin, sectioned, and stained with H&E.

Pulmonary endothelial cell activation was studied in isolated cells by flow cytometry. Mice were euthanized using sodium pentobarbital. Lungs were inflated with an enzymatic digestion buffer (DMEM, 1 mg/ml collagenase type IV [Invitrogen], and 0.2 mg/ml DNase I [Sigma-Aldrich]), after which they were dissected away from the trachea and heart and incubated in 5 ml of enzymatic digestion buffer in a 50-ml conical tube for 30 min at 37°C under agitation at 200 rpm. After the 30-min incubation, 25 ml of PBS was added, and the samples were vortexed for 30 s. The resulting cell suspension was passed through a 70- μ m filter and washed in PBS. RBCs were lysed using Gey's solution and washed in PBS/2% FCS, after which cells were counted and resuspended for flow cytometry experiments.

For flow cytometry, nonspecific Ab binding was blocked by incubating 1×10^6 cells with Fc Block anti-CD16/32 (BD Biosciences, no. 553141). After washing, cells were stained at 4°C in PBS/2% FCS containing 0.1% sodium azide. Reagents and Abs used in these experiments were as follows: Live/Dead (1:500; Invitrogen, no. L23105), CD45-FITC (1:400; eBioscience, no. MCD4501), CD11c-PE-Cy7 (1:200; BD Biosciences, clone HL3, no. 561022), CD11b-eFluor 450 (1:800; eBioscience, clone MI/70, no. 48-0112-82), Ly6G-Alexa Fluor 700 (1:500; BD Biosciences, clone 1A8, no. 561236), CD45-BB700 (1:6400; BD Biosciences, no. 566440), CD326-BV605 (1:500; BD Biosciences, no. 740389), CD31-FITC (1:400; BD Biosciences, no. 558738),

CD141-BV421 (1:800; BD Biosciences, no. 747647). Data were collected on a BD LSR II flow cytometer (BD Biosciences) and analyzed using FlowJo (Tree Star, Ashland, OR). Ab titration experiments were performed to determine the Ab concentration resulting in the best separation of cell populations and minimize nonspecific binding under the same experimental conditions.

Pulmonary vascular barrier permeability to solutes was assessed by measuring extravasation of FITC-labeled 70-kDa dextran. For these studies, mice were reanesthetized 24 h after experimental treatment, and then given a retro-orbital injection of 70-kDa FITC-dextran (100 μ l of 3 mg/ml). After 30 min, they were euthanized with transcardial perfusion with PBS to eliminate any remaining FITC-dextran in circulation. Lungs were isolated and homogenized in 1 ml of RIPA buffer and centrifuged at 12,000 \times g for 20 min. The concentration of 70-kDa FITC-dextran in the supernatant was detected via fluorescence measurement (excitation 490 nm, emission 520 nm) and interpolation from a standard curve of known concentrations of FITC-dextran. Results are presented as nanograms of FITC-dextran per milligram of protein in the supernatant.

Ex vivo studies on intact murine arteries

Third-order branches of mesenteric arteries were isolated from wild-type C57BL/6J mice. Surrounding tissue was removed and single mesenteric arteries were mounted onto size-matched glass cannulae in an arteriograph chamber (Living Systems Instrumentation, St. Albans, VT) as previously described (20). The proximal pipette was attached to a servo-controlled, pressure-regulating device (Living Systems Instrumentation). The mesenteric arteries were then pressurized to 80 mm Hg in 37°C physiological saline solution (120 mM NaCl, 4.7 mM KCl, 1.2 mM KH_2PO_4 , 1.2 mM MgCl_2 , 2.5 mM CaCl_2 , 7.5 mM glucose, 20 mM NaHCO_3 , pH 7.4) continuously equilibrated with bioair of the following composition: 20% O_2 and 5% CO_2 in 75% N_2 . Pressurized mesenteric arteries were visualized with an inverted light microscope equipped with a charge-coupled device camera and edge-detection software for continuous monitoring of internal mesenteric artery diameter (IonOptix, Milton, MA). Mesenteric arteries were treated with Ca^{2+} -free physiological saline solution at the conclusion of each experiment to obtain maximal dilation diameter. Histones (1, 10, and 100 $\mu\text{g/ml}$) or saline (control) were delivered through the cannula into the lumen of the mesenteric arteries. Conditions of low shear stress were used to avoid stimulating flow-mediated vasodilatory mechanisms (~ 2 $\mu\text{l/min}$ flow, < 5 dyne/ cm^2). Endothelial cell function was determined by measuring the dilatory response to activation of endothelial small conductance and intermediate conductance Ca^{2+} -activated potassium channels with 1 μM NS309.

Calcium imaging in pulmonary arteries ex vivo

Calcium imaging in the native endothelium of mouse pulmonary arteries was performed as previously described (46). Briefly, fourth-order (~ 50 μm) pulmonary arteries were pinned down on face on a Sylgard block and loaded with Fluo-4-AM (10 μM) in the presence of pluronic acid (0.04%) at 30°C for 30 min. Fluo-4 was excited at 488 nm with a solid-state laser and emitted fluorescence was captured using a 525/36-nm band-pass filter. Images were acquired at 30 frames per second with an Andor Revolution WD (with Borealis) spinning-disk confocal imaging system (Oxford Instruments, Abingdon, U.K.) comprised of an upright Nikon microscope with a 60 \times water dipping objective (numerical aperture 1.0) and an electron multiplying charge-coupled device camera (iXon 888, Oxford Instruments, Abingdon, U.K.). Ca^{2+} signals were analyzed using the custom-designed SparkAn software (46, 47). A region of interest defined by a 1.7- μm^2 (5×5 pixels) box was placed at a point corresponding to peak event amplitude to generate a fractional fluorescence (F/F_0) trace. F/F_0 traces were filtered using a Gaussian filter and a cutoff corner frequency of 4 Hz. The number of Ca^{2+} events was autodetected using a detection threshold of 0.3 F/F_0 in SparkAn (custom software, Dr. Adrian Bonev, Burlington, VT). Each data point indicates one field of view from one pulmonary artery. Calf thymus histones containing H1, H2a, H3, and H4 histones (unfractionated histones) were used for these experimental series.

Histone-mediated cytotoxicity assay in cultured cells

The cytotoxicity of calf-thymus histones and citrullinated histone H3 was determined on mouse lung microvascular endothelial cells (Cell Biologics, no. C57-6011) using propidium iodide (PI). Cells were treated with various concentrations of histones or citrullinated histone H3 and then incubated with PI (2 $\mu\text{g/ml}$) for 20 min at 37°C. Then, PI fluorescence was quantified using a microplate reader and dead cells were visualized under a confocal microscope.

Calibrated automated thrombinography in cultured cells

Human endothelial cells (EA.hy926; ATCC CRL-2922) were incubated with histones (50 $\mu\text{g/ml}$), suramin (50 μM), histones + suramin, or DMEM alone for 4 h at 37°C, 5% CO_2 . Calf thymus histones containing H1, H2a, H3,

and H4 histones (unfractionated histones) were used for these experimental series. The cells were released from the tissue culture wells with trypsin and subjected to centrifugation (170 \times g, 7 min). Cell pellets were washed once by resuspension in 20 mM HEPES, 0.15 M NaCl (pH 7.4) (HBS) followed by centrifugation. The final cell pellets were resuspended in HBS and adjusted to a final concentration of $1 \times 10^7/\text{ml}$.

Thrombin generation was assessed using a modified calibrated automated thrombogram. Plasma was thawed at 37°C in the presence of corn trypsin inhibitor (0.1 mg/ml final concentration) and incubated with the thrombin substrate Z-Gly-Gly-Arg 7-amido-4-methylcoumarin hydrochloride (0.42 mM) (Bachem, Bubendorf, Switzerland) and CaCl_2 (15 mM) (3 min, 37°C). The reactions were initiated by the addition of relipidated tissue factor (TF)_{1–242} (6.5 pM) (a gift from Dr. R. Lunblad, Baxter Healthcare) and synthetic vesicles consisting of 80% phosphatidylcholine and 20% phosphatidylserine (PCPS) (20 μM), or EA.hy926 cells (2×10^5). Fluorescence was measured (excitation of 370 nm, emission of 460 nm) for 1 h with a Cytation 3 imaging reader (BioTek, Winooski, VT). Changes in fluorescence were converted to thrombin concentrations using a calibration curve created from sequential dilutions of human thrombin. If no change in fluorescence was noted after 60 min, the lag time for the sample was defined as > 60 min.

Fluorescence spectroscopy

Fluorescence spectroscopy was used to determine the equilibrium K_d values for the histone/suramin complex. Calf thymus histones containing H1, H2a, H3, and H4 histones (unfractionated histones) or citrullinated histone H4 (Cayman Chemical, no. 17926) were used for binding experiments. The changes in intrinsic suramin fluorescence emission were measured with a microplate reader (BioTek, Winooski, VT) at 25°C. The samples were excited at 315 nm and the emission spectrum was measured between 370 and 480 nm. Histones did not show spectral overlap in that range (Supplemental Fig. 1A). The titration was performed stepwise with a suramin stock concentration (1 μM) in assay buffer containing 50 mM HEPES, 100 mM NaCl, and 2 mM CaCl_2 (pH 7.4); fluorescence measurements were performed after each titration with histones (0–8 μM). After normalization of the fluorescence emission signal, the K_d for each suramin/histones complex was estimated by nonlinear curve fitting with a sigmoidal dose–response function using GraphPad 7 software (GraphPad Software, San Diego, CA). The percentage of bound suramin/histones was plotted against the concentration of free histones.

Molecular modeling

Model preparation. All of the models were constructed using the Desmond/Maestro program (v2016-3, Schrödinger) using the System Builder in Maestro. Each model contained a complete histone octamer (PDB: 5XF3) with or without DNA and six suramin molecules that were arbitrarily placed at a minimum distance of 15 Å from the proteins. The SPC (simple point-charge) water model was employed to solvate the complexes, with counterions and 0.12 M NaCl, 0.047 M KCl, 0.025 M CaCl_2 , and 0.012 M MgCl_2 . The construct with a DNA-bound histone has a total of 197,122 atoms in a periodic box of $\sim 123 \times 128 \times 127$ Å³, whereas the one with a DNA-free histone has 180,860 atoms in a box of $\sim 120 \times 122 \times 124$ Å³.

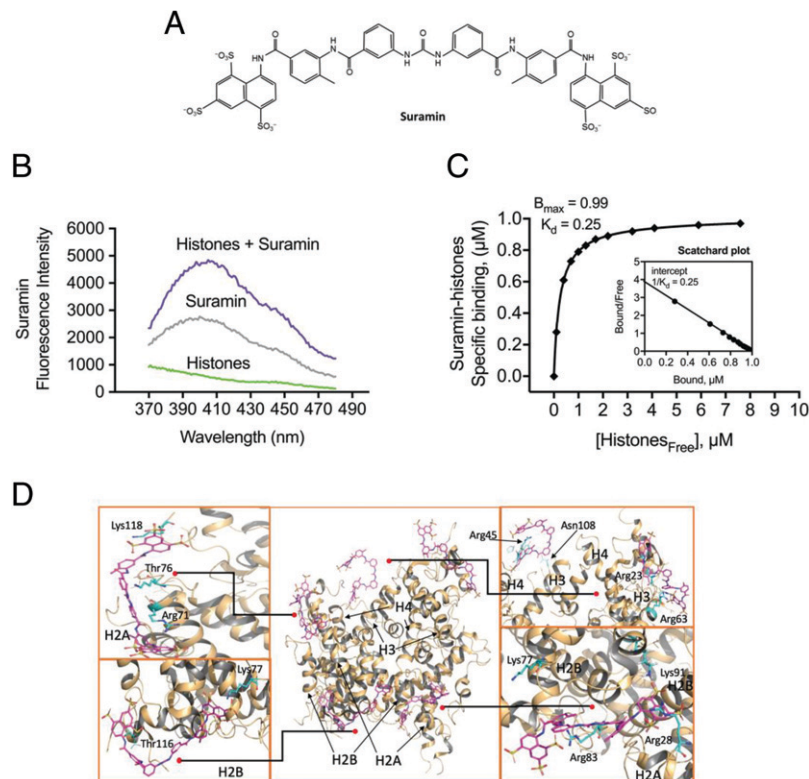
Simulation setup. All simulations were performed in the Desmond program with the OPLS3 force field in the NPT ensemble (1.01325 bar, 310 K, Martyna–Tobias–Klein coupling scheme) with a time step of 2 fs (48, 49). The particle mesh Ewald technique was used for the electrostatic calculations. The van der Waals and short-range electrostatics were cut off at 9.0 Å. Hydrogen atoms were constrained using the SHAKE algorithm. Each simulation had two 700-ns replicas.

Visualization and analysis. PyMOL (v2.5, Schrödinger) and Visual Molecular Dynamics (VMD, <http://www.ks.uiuc.edu/Research/vmd/>) were used for the structure visualization of the simulations; the simulation analysis panel was carried out in Maestro.

Statistical analysis

Datasets were first tested for normal distribution using the Kolmogorov–Smirnov method to determine the appropriate parametric or nonparametric test with which to proceed. Data were analyzed by a two-tailed unpaired or paired Student *t* test, Mann–Whitney *U* test, Wilcoxon rank test, one-way or two-way ANOVA and Bonferroni post hoc test, or the Mantel–Cox test for survival using GraphPad Prism 7.04 (GraphPad Software, La Jolla, CA). A *p* value < 0.05 was considered statistically significant.

FIGURE 1. Suramin binds histones in solution. **(A)** Chemical structure of suramin. **(B)** In vitro fluorescent spectroscopy studies were used to biochemically establish the interaction between suramin and histones. We established the absorbance and emission spectra for histones and suramin in solution (Supplemental Fig. 1A), and then measured suramin sodium salt-intrinsic fluorescence using increasing concentrations of suramin to determine the saturation range of the detector (Supplemental Fig. 1B). **(C)** Scatchard plot analysis of the binding curve demonstrates a single high-affinity binding site with a K_d of 250 nM ($n = 3$ replicates for binding studies). **(D)** Molecular dynamics simulations showing interactions between suramin molecules and the histone octamer in solution. Several exposed amino acid residues including arginine, asparagine, lysine, and threonine form hydrogen bonds with the sulfate groups on suramin (Lys¹¹⁸, Thr⁷⁶, Arg⁷¹, Lys⁷⁷, Thr¹¹⁶, Arg⁴⁵, Asn¹⁰⁸, Arg²³, Arg⁶³, Lys⁹¹, Arg⁸³, Arg²⁸). These include residues on H2A, H2B, H3, and H4, which are predicted to form stable electrostatic interactions with the sulfate groups on suramin.



Results

Suramin binds to individual histones in solution and decreases histone-mediated cytotoxicity

Based on its molecular structure, we hypothesized that suramin, a highly charged polysulfonated naphthylurea, would bind avidly to cationic histone complexes (Fig. 1A). When NETs or nucleosomes enter the bloodstream, they are exposed to endogenous nucleases that rapidly digest DNA, leaving free histone proteins (15). Therefore, we focused on testing the interactions between suramin and histones. First, fluorescence spectroscopy studies were used to biochemically establish the K_d and number of high-affinity binding sites for interactions between the two molecules. We established the absorbance and emission spectra for histones and suramin in solution and then measured suramin sodium salt-intrinsic fluorescence using an excess of suramin in the presence of increasing concentrations of histones (Fig. 1B, Supplemental Fig. 1). The resulting interactions are represented using a binding curve (Fig. 1C). Scatchard analysis of the binding curve demonstrates a single high-affinity binding site with a K_d of 250 nM (Fig. 1C). These results confirm that suramin readily binds histones in solution. We then used all-atom molecular dynamics simulations to determine likely interactions between suramin molecules and the histone octamer in solution (Fig. 1D, Supplemental Video 1). Suramin quickly formed electrostatic contacts between its SO_3^- and arginines on the protein surface such as Arg⁵³ and Arg⁶⁹ of H3, Arg²³ and Arg⁴⁵ in H4, Arg¹⁷ in H2A, and Arg³⁰ in H2B. Hydrogen bonding between suramin and several threonines was also observed, such as Thr⁸⁰ of H3, Thr¹⁶ and Thr⁷⁶ in H2A, and Thr¹¹⁶ in H2B. These interactions remained stable toward the end of our simulations and enabled steady binding for five of the suramin molecules to histones. Additionally, we tested the interaction between citrullinated H3 and suramin. Binding experiments by fluorescence spectroscopy revealed no changes of the citrullinated H3 fluorescence peak in the presence of suramin, indicating a lack of binding (Supplemental Fig. 2A). We next studied whether suramin affects cytotoxicity induced by either individual histones or citrullinated H3 by PI staining. Suramin

significantly decreased cell death induced by 100 $\mu\text{g/ml}$ histones, whereas treatment with suramin did not protect against citrullinated H3 (Supplemental Fig. 2B, 2C). These results further suggest that suramin binds to individual histones preventing endothelial cell cytotoxicity but does not bind as effectively to NET-derived histones.

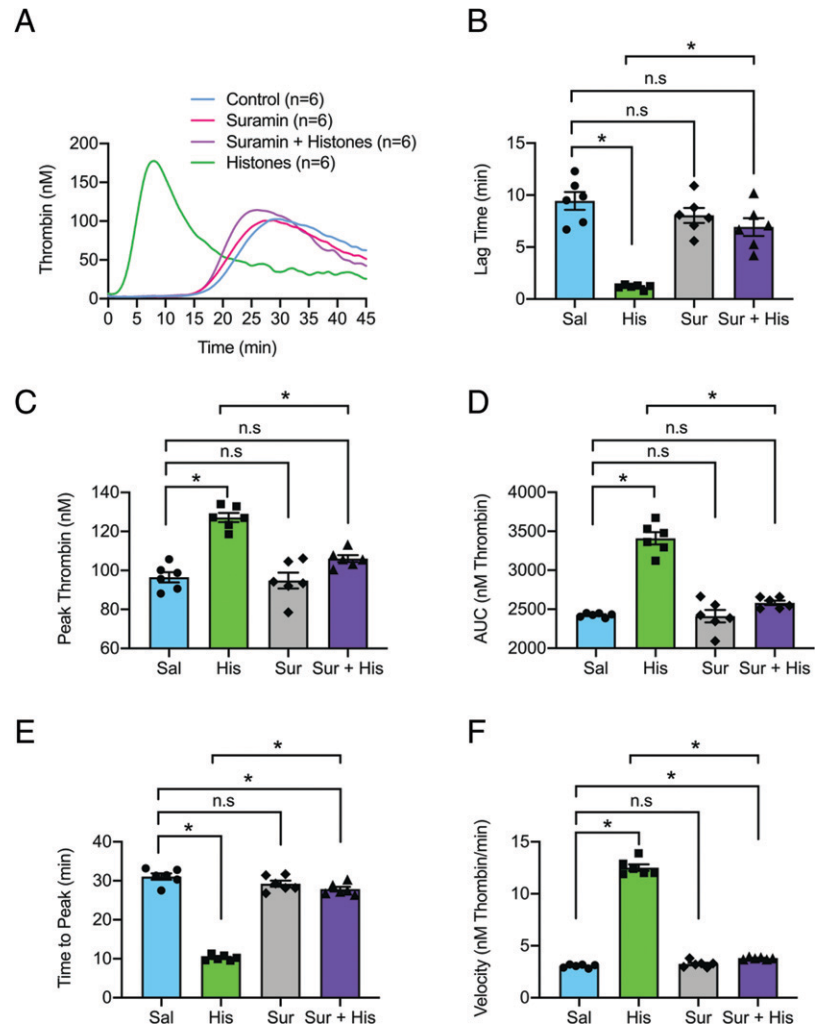
Histones induce rapid thrombin generation on human endothelial cells that is blocked by suramin

Thrombin is the ultimate protease in the clotting cascade, catalyzing fibrin formation. The formation of thrombin following cleavage of prothrombin is rate limiting to the coagulation process (50). Phosphatidylserine-dependent prothrombin activation on the endothelial surface leads to the formation of microthrombi, shedding of extracellular vesicles and glycocalyx, neutrophil migration, and efflux of water into damaged interstitial tissues (10, 50). Extracellular vesicles, enriched with histones, have procoagulant membranes and carry microRNAs into the bloodstream (51). To test whether histones promote thrombin generation, we used calibrated automated thrombograms in recalcified pooled healthy human plasma, in the absence of exogenous TF and phospholipid membrane, to measure the ability of cultured human endothelial cells (Ea.hy926) to support thrombin production. Under these conditions, thrombin formation occurred slowly (lag time >15 min), but when histones were applied, thrombin generation was accelerated, with a lag time of <5 min (Fig. 2A, 2B). Histone treatment also had prothrombotic effects on other measures of thrombin generation including peak thrombin, endogenous thrombin potential, time to peak thrombin, and the rate of thrombin generation (Fig. 2C–F). In the presence of suramin, measures of histone-induced thrombin generation were significantly ameliorated to levels observed in untreated cells.

Suramin prevents disruption of endothelial-dependent vasodilation and endothelial cell calcium overload caused by histones

Endothelial-dependent vasodilation of small arteries in response to NO and other hyperpolarizing stimuli is essential for the regulation of regional blood flow to meet metabolic demands. Disruption of

FIGURE 2. Histones drive rapid thrombin generation on human endothelial cells that is blocked by suramin. **(A)** Calibrated automated thrombogram tracings of thrombin generation (nanomolars) versus time (minutes) by cultured human endothelial cells (Ea.hy926) in recalcified, pooled, healthy human plasma. Histones (50 μ g/ml), suramin (50 μ M), or a combination of both were exogenously added to the cell culture and plasma samples as needed. **(B)** Summary data for lag time in control (9 ± 0.8 min; $n = 6$), suramin (8 ± 0.7 min; $n = 6$), suramin and histones (67 ± 0.9 min; $n = 6$), and histones (1 ± 0.1 min; $n = 6$) samples. **(C)** Summary data for peak thrombin in control (96 nM; $n = 6$), suramin (94 ± 4 nM; $n = 6$), suramin and histones (106 ± 2 nM; $n = 6$), and histones (127 ± 2 nM; $n = 6$) samples. **(D)** Summary data for area under the curve (AUC; nanomolars thrombin) in control ($143,732 \pm 2,498$ nM; $n = 6$), suramin ($139,915 \pm 2,355$ nM; $n = 6$), suramin and histones ($147,896 \pm 2,968$ nM; $n = 6$), and histones ($180,248 \pm 3,977$ nM; $n = 6$) samples. **(E)** Summary data for time to peak in control (31 ± 0.8 min; $n = 6$), suramin (29 ± 0.8 min; $n = 6$), suramin and histones (28 ± 0.6 min; $n = 6$), and histone samples (10 ± 0.3 min; $n = 6$). **(F)** Summary data for velocity in control (3.0 ± 0.1 nM thrombin/min; $n = 6$), suramin (3.2 ± 0.1 nM thrombin/min; $n = 6$), suramin and histones (3.8 ± 0.04 nM thrombin/min; $n = 6$), and histones (13 ± 0.3 nM thrombin/min; $n = 6$) samples. Data are expressed as mean \pm SEM. * $p < 0.05$, by ordinary one-way ANOVA with Bonferroni's correction for multiple comparisons. A new biological replicate culture well was used for each group.



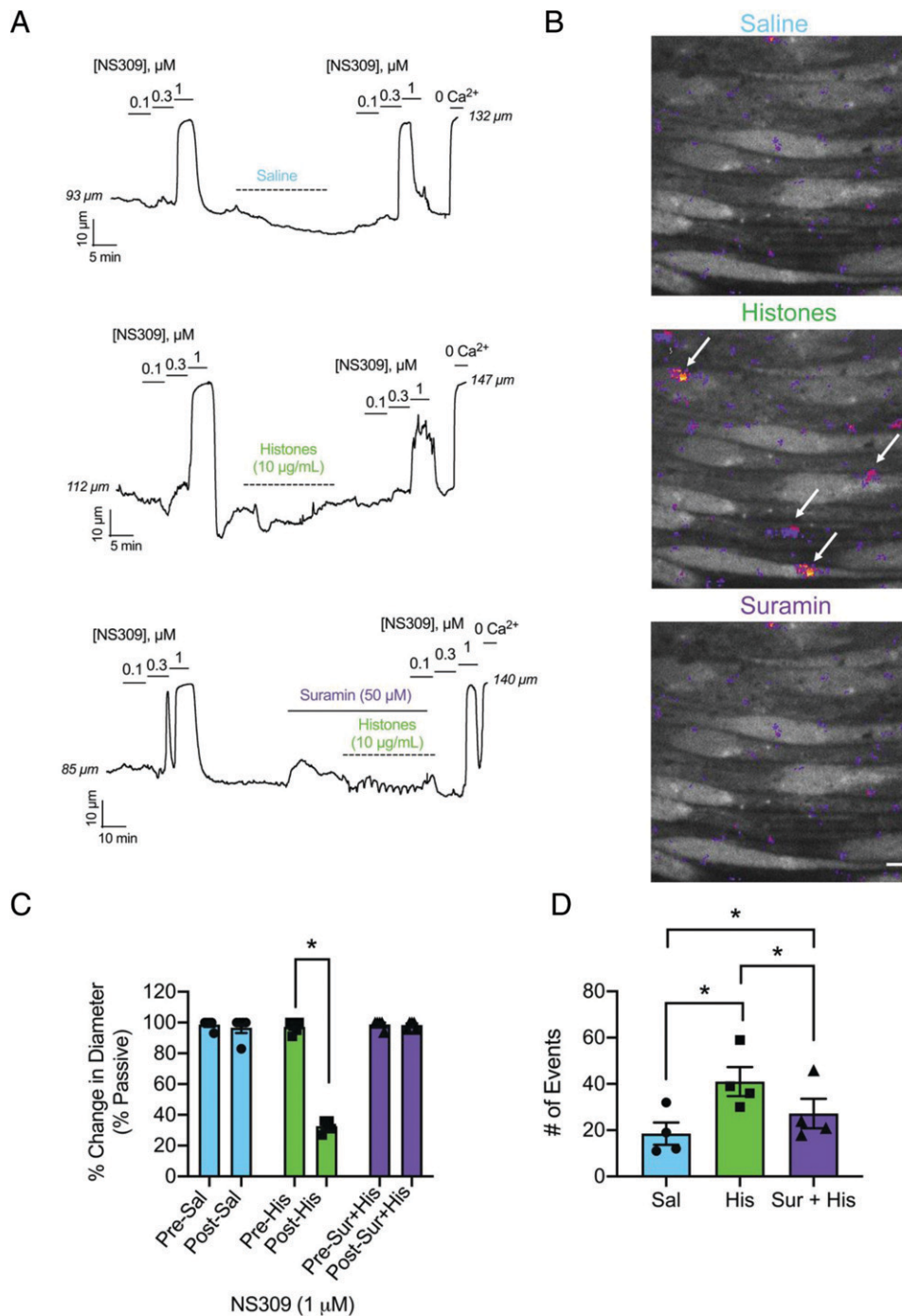
endothelial-dependent vasodilation is considered the hallmark of endothelial dysfunction. We previously demonstrated that histones induce aberrant endothelial cell calcium responses that disrupt normal vasodilatory signals in small mesenteric arteries (20, 47). In this study, we used video-edge detection to record the vasodilatory responses of pressurized, resistance-sized arteries from the mouse mesenteric circulation to the exposure of the endothelial-dependent vasodilator NS309 (0.1–1 μ M) before and after intraluminally perfusing histones (10 μ g/ml) through the vessel in the presence and absence of suramin (50 μ M) (Fig. 3A, 3B). Vasodilation to 1 μ M NS309 after 30 min of histone exposure was reduced to 33% of the prehistone control dilation. Vasodilatory function was completely preserved during this same experiment while in the presence of suramin (50 μ M). Because lung injury is a significant concern in conditions characterized by high levels of histones such as acute respiratory distress syndrome (19), we also studied vascular preparations from small mouse pulmonary arteries. These blood vessels were surgically opened on one side to expose the endothelial cell layer for direct measurement of a fluorescent calcium indicator using confocal microscopy (Fig. 3C, 3D). Similar to our prior findings in human and mouse mesenteric arteries (20), we found that histones (10 μ g/ml) significantly increased the number of detectable calcium events compared with baseline. The presence of suramin (50 μ M) during histone application significantly decreased the number of calcium events; however, the activity was still elevated when compared with the baseline control (Fig. 3D). Together, pretreatment with suramin completely prevents histone-induced endothelial vasodilatory

dysfunction in pressurized arteries and significantly decreases aberrant calcium signaling caused by exposure to histones.

Suramin prevents adhesion molecule expression, neutrophil recruitment, and pulmonary endothelial barrier disruption caused by histones

The results of our biochemical and in vitro work provided a rationale for an in vivo model of histone toxicity. Circulating histones can injure platelets, erythrocytes, and vascular endothelial cells from multiple tissue beds. However, in humans and animal models of trauma, lung tissue is particularly vulnerable to circulating damage-associated molecular pattern proteins (19). Therefore, we next tested the hypothesis that suramin would prevent the increase in circulating biomarkers, endothelial cell activation, and influx of inflammatory cells into the lungs caused by histone infusion (45 mg/kg). To specifically assess the endothelial effects of suramin after histone exposure, we freshly isolated mouse pulmonary endothelial cells and measured their adhesion molecules using flow cytometry. The extent of neutrophil migration into the lungs after histone exposure was also quantified. After 24 h, lung tissue was dissociated, and the frequency of neutrophils was determined by expression of CD11b and Ly6G by flow cytometry. Treatment with histones resulted in a statistically significant increase in the frequency of neutrophils in the lung (Supplemental Fig. 3A, 3B). Lung endothelial cell ICAM-1 expression was also significantly increased by histones (Supplemental Fig. 3C, 3D). Suramin ameliorated these histone-induced effects, causing a significant reduction in the frequency of neutrophils and expression of endothelial cell ICAM-1.

FIGURE 3. Suramin prevents endothelial dysfunction and calcium overload caused by histones. **(A)** Representative tracings of pressurized (80 mm Hg), third-order, mouse mesenteric arteries. Histones (10 µg/ml) or saline (control) was flowed through the lumen at 2 µl/min (<5 dyn/cm²) for 30 min. Dilations to the endothelial-dependent vasodilator NS309 (0.1, 0.3, and 1 µM) preflow and postflow were recorded. In one subset of experiments suramin (50 µM) was superfused abuminally for 10 min prior to and then continuously during histone flow. Maximal dilations were elicited at the end of the experiments using Ca²⁺-free buffer (0 Ca²⁺) physiological saline solution. **(B)** Representative images from en face mouse pulmonary arteries loaded with Fluo-4 (10 µM) on a spinning disk confocal microscope. All images are from the same field of view recorded over 2 min. Arrows indicate large histone-induced calcium event F/F₀ regions of interest. Scale bar, 10 µm. **(C)** Paired summary data of percent dilation to 1 µM NS309 preflow and postflow of saline (Pre-Sal 99 ± 1 versus Post-Sal 97 ± 3%; n = 5; n.s.), histones (10 µg/ml) (Pre-His 97 ± 2 versus Post-His 33 ± 2%; n = 5; *p < 0.05, by paired Student *t* test), and suramin (50 µM) with histones (Pre-Sur+His 99 ± 1 versus Post-Sur+His 98 ± 1%; n = 5; n.s.). **(D)** Summary data of the paired total number of events per field after saline (control; 19 ± 5 events; n = 4), histones (His; 10 µg/ml; 41 ± 6 events; n = 4), and suramin (50 µM) and histones (Sur+His; 27 ± 6 events; n = 4) application. Significant differences were determined using a repeated measures one-way ANOVA test with a Holm–Sidak correction for multiple comparisons for all three groups; *p < 0.05. Data are represented as mean ± SEM. A new biological replicate was used for each arteriography and calcium imaging experiment.



Suramin prevents lung injury and improves survival after exposure to histones

To assess clinically relevant outcomes, we next tested whether suramin would prevent death and lung injury in vivo after histone exposure. We randomized mice to one of four experimental groups: saline; saline and histones (75 mg/kg); suramin (20 mg/kg) and histones; or suramin (50 mg/kg) and histones (Fig. 4A). Survival was monitored and updated every minute for the 35-min duration of the study. Groups were compared using a Mantel–Cox analysis and Mantel–Haenszel for the hazard ratio. Of animals receiving 75 mg/kg histones alone, 70% died abruptly within 10 min and showed symptoms such as bleeding from the nose, pink frothy sputum, and signs of respiratory distress, and only 20% survived the 35-min period. In contrast, 100% of animals receiving suramin at the higher dose of

50 mg/kg with the lethal dose of histones survived when compared with the histone group (1.959–35.09, 95% confidence interval [CI]; 8.29 hazard ratio; p < 0.05). The lower dose of suramin (20 mg/kg) also provided a modest survival benefit (36%) when compared with the high dose (1.359–28.71, 95% CI; 6.25 hazard ratio; p < 0.05) but not to the histone-only group (0.9702–9.410, 95% CI; 2.49 hazard ratio; not significant). In a separate set of mice exposed to histone infusion (45 mg/kg) in the presence or absence of the higher dose of suramin (50 mg/kg), we found that suramin reversed intra-alveolar hemorrhage visible on histology as well as elevation in cell counts and protein measured in BALF (Fig. 4B, 4C). As an additional control, we also examined lung sections from mice receiving suramin alone (50 mg/kg). These were indistinguishable from mice treated with saline (Supplemental Fig. 4A). Pulmonary barrier breakdown

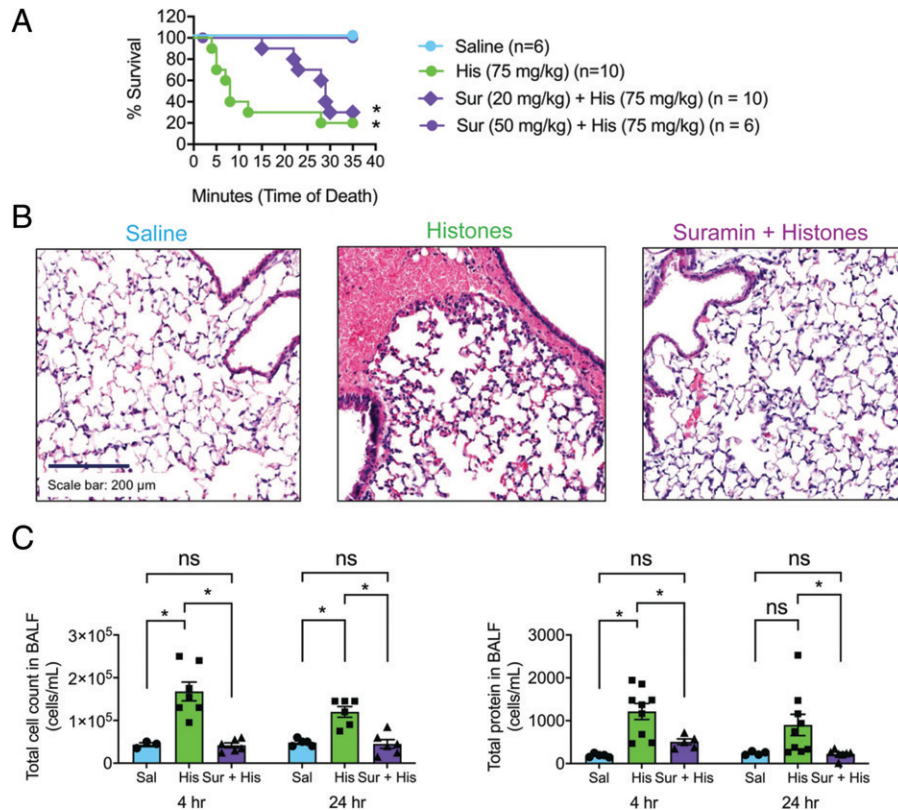


FIGURE 4. Suramin improves survival and prevents lung injury and edema caused by histones. **(A)** Saline (control; $n = 6$), a lethal dose of histones (His; 75 mg/kg; $n = 10$), and a lethal dose of histones with suramin (Sur+His; 20 mg/kg, $n = 11$ or 50 mg/kg, $n = 6$) were injected into mice and survival was recorded during the course of 35 min. Suramin was injected i.p. $*p < 0.05$ for each group compared with saline (by a Mantel–Cox test) **(B)** Representative images of H&E stain of a histological section of paraffin-embedded fixed lung tissue from a mouse from saline-, histone-, and suramin + histone-treated groups ($n = 3$). The dark blue color denotes cell nuclei, light pink indicates the extracellular matrix, and red indicates erythrocytes. Scale bar, 200 μm . **(C)** Summary data of the total, nondifferentiated cell counts in the bronchoalveolar lavage fluid (BALF) at 4 h after saline (control; $43,333 \pm 4,410$ cells/ml; $n = 3$), histones (His; 45 mg/kg; $167,847 \pm 22,008$ cells/ml; $n = 7$), or suramin (50 mg/kg and histone injection (Sur+His; $41,667 \pm 5,725$ cells/ml; $n = 6$) and 24 h after saline (control; $48,000 \pm 3,742$ cells/ml; $n = 5$), histones (His; 45 mg/kg; $120,000 \pm 12,649$ cells/ml; $n = 6$), or suramin (50 mg/kg) and histone injection (Sur+His; $45,000 \pm 10,247$ cells/ml; $n = 6$). Summary data for the total protein leakage into the BALF at 4 h after saline (control; 188 ± 19 $\mu\text{g/ml}$; $n = 5$), histones (His; 45 mg/kg; 1215 ± 186 $\mu\text{g/ml}$; $n = 9$), or suramin (50 mg/kg) and histone injection (Sur+His; 507 ± 66 $\mu\text{g/ml}$; $n = 5$) and 24 h after saline (control; 239 ± 21 $\mu\text{g/ml}$; $n = 5$), histones (His; 45 mg/kg; 901 ± 249 $\mu\text{g/ml}$; $n = 9$), or suramin (50 mg/kg) and histone injection (Sur+His; 225 ± 39 $\mu\text{g/ml}$; $n = 7$). Data are expressed as mean \pm SEM. $*p < 0.05$, by two-way ANOVA with Bonferroni's correction for multiple comparisons. A new biological replicate was used for each survival study experimental group, H&E staining ($n = 3$ for each group), cell counts, and total protein in BALF measurements.

induced by histones, quantified as the extravasation of 70-kDa FITC-labeled dextran, was significantly decreased by suramin. Suramin also blocked extravasation of the labeled dextran in renal tissue caused by histones (Supplemental Fig. 4B).

Discussion

Histones, released from injured cells or in NETs extruded from activated neutrophils, can activate and damage vascular cells through several mechanisms that are not fully understood. Histones can activate ion channels, observed by membrane potential and current recordings in endothelial cells and other cells (19, 52, 53). With prolonged exposure (minutes to hours), or at high concentrations, histones, and histone H4 in particular, can also damage lipid bilayers in any cell type, including endothelial cells, and act as cell-penetrating proteins (11, 22, 31). Histones can also engage innate immune responses leading to prothrombotic activation of endothelial cells (27, 54, 55) or pyroptosis (6, 24–26). All of these mechanisms can contribute to acute endotheliopathy. In the current study, we looked at the interaction between extracellular histones and suramin and demonstrated that not only does suramin form a stable complex with histone proteins, but, also, this neutralizing effect completely prevents histone-induced endothelial dysfunction and mortality.

Furthermore, we also explored the interaction between NET-derived histones (i.e., citrullinated histones) and suramin. We found that citrullination, an important posttranslational modification on histones essential for the formation of NETs, prevents the interaction between citrullinated histones and suramin. The loss of charge on NET-derived histones most likely decreases the binding force between citrullinated histones and suramin, and therefore suramin's chelating (protecting) effect. Suramin has been used for >100 y as an antiparasite and anticancer agent, and, importantly, is considered among the safest and most effective drugs for health care by the World Health Organization. This discovery of a new mechanism of action for a widely available and easily administered drug, as a blocker of deleterious histone effects, provides a tantalizing target for the potential clinical therapeutic use of suramin in acute immunovascular and thromboinflammatory conditions.

Our results provide new insight into the pathophysiological outcomes of histone-induced organ injury. We provide (to our knowledge) the first demonstration that in native, pulmonary artery preparations, histones elicit calcium-mediated events similar to those we previously observed in mesenteric resistance arteries from humans and mice. We also found that histone infusion caused endothelial barrier breakdown of small blood vessels in both kidney and lung, with

increased extravasation of the 70-kDa dextran, but not in brain. This is consistent with other evidence that pulmonary and renal (6, 17, 19) tissue beds are highly sensitive to histone-induced injury. It was recently shown that histones increased paracellular permeability in the hippocampus but not cortical brain regions (23). It is possible that we missed these regional cerebrovascular effects because we quantified vascular leak for the entire brain and not specific regions, or because we used a 70-kDa tracer rather than a smaller sized dextran that would more specifically target blood–brain barrier permeability. In the current study, our focus was on lung injury, with results in freshly harvested lung cells, isolated vascular preparations, and in vivo models uniformly supporting the model in which histones activate endothelial cells to increase cellular adhesion molecule expression, in conjunction with increased release of circulating adhesion molecules. These changes in the pulmonary vascular endothelium result in increased neutrophil recruitment to the lungs.

Importantly, we also demonstrate a new, endothelial-dependent mechanism by which histones increase thrombosis. Prior studies have shown that histones can increase plasma thrombin generation in purified systems by reducing thrombomodulin-dependent protein C activation (56). In this study, we provide new evidence (to our knowledge) that histones can rapidly activate endothelial cells directly to promote thrombin generation. We show that on endothelial cells, in the absence of added TF or phospholipids, thrombin formation occurs slowly, but when histones are applied, thrombin generation is accelerated, with a lag time of <5 min. This reaction was blocked by suramin. The time course of this reaction, occurring minutes after histone exposure, was unexpected, since known procoagulant responses of endothelial cells to histones, such as release of von Willebrand factor (54), upregulation of TF (27), or downregulation of thrombomodulin mRNA and surface Ags (55), which occur 1–8 h after exposure. Thus, rapid phosphatidylserine translocation, possibly due to TMEM16f activation (57, 58), coupled with mobilization of “cryptic” TF in the endothelial cell membrane, likely drives the rapid reactions we observe. Understanding the effectors of rapid procoagulant responses to histones may improve targeted therapies to protect against excessive thrombosis in inflammatory conditions.

Suramin offers several advantages over other therapeutic strategies to prevent histone-mediated vascular injury. Polyanions such as heparin can neutralize histones and prevent histone-mediated cytotoxicity (42, 59–61). Heparin improves outcomes in some patients with sepsis (59) or COVID-19 (62, 63), but the mechanisms are not fully understood. Furthermore, heparin cannot be safely used in all patients, such as those requiring surgical procedures, because of the risk of hemorrhagic bleeding. Unlike heparin, which requires continuous infusion, suramin dosing for acute inflammatory conditions is infrequent (once per week), and extensive experience with this drug has shown that it has an excellent safety profile. Anticoagulant effects have been demonstrated in trials of continuous infusions of suramin after 14 d, but single injections of suramin do not impact blood clotting (64). It is also readily available worldwide, at a low cost. Other naturally occurring substances, such as pentraxin 3 (65), activated protein C (35), C1 esterase inhibitor (66), and inter- α inhibitor proteins (39), as well as anti-histone Abs (3, 4, 42) and synthetic polyanions (22, 44), can also neutralize excessive histones to prevent toxicity, but these drugs are either not approved or not available for human use. Albumin or fresh-frozen plasma may have benefits in trauma and sepsis, in part due to histone binding (67), but blood products are limited resources with high costs compared with suramin.

Taken together, these results provide evidence supporting the use of suramin in trauma and sepsis. This is particularly important in the context of the unprecedented global public health crisis caused by the novel SARS-CoV-2 virus, because histone levels are elevated in individuals with COVID-19 (18, 68), and endotheliopathy and

thromboinflammation secondary to NETs drive progression from systemic inflammation to organ failure and death (1, 2). Of note, suramin may have other mechanisms of therapeutic action in viral illness. Polyanion inhibitors have been used to block viruses that require cell surface sugars such as heparan sulfate to infect humans, which include HIV, Ebola, Zika, and SARS-CoV-2. These inhibitors include naturally occurring therapeutic polyanions such as heparin, synthetic polyanions, such as suramin, or modified cyclodextrins (69). Heparin is the subject of over a dozen registered clinical trials for SARS-CoV-2 (<https://clinicaltrials.gov>) and has efficacy in COVID-19 (63). Most of these trials are testing injectable unfractionated heparin or low-molecular mass heparin at prophylactic or therapeutic anticoagulant doses. Other trials are using intranasal or nebulized heparin in an attempt to block viral entry, because heparin can serve as a decoy for the target cell heparan sulfate needed for optimal interaction between viral spike protein and ACE2. Heparin is also believed to have immunomodulatory and endothelial protective effects, based on evidence of prior benefit in sepsis from other causes, and histone binding may be an important therapeutic mechanism of action for heparin (59, 70). Suramin is a competitive inhibitor of heparin, and it has been suggested, but not established, that suramin shares a mechanism of action against SARS-CoV-2 by acting as a decoy for heparan sulfate that can block spike protein and ACE2 interactions (71). Suramin also inhibits the main protease needed for SARS-CoV-2 infection (72), and it is the subject of at least one COVID-19 clinical trial at the time of this submission (<https://clinicaltrials.gov>).

Although our data demonstrate that direct interaction and neutralization of histone proteins is a mechanism of action for suramin, we did not rule out the possibility that the drug has other mechanisms that might contribute to endothelial protection. For example, previous studies have demonstrated mechanisms of action for suramin, including known effects on many enzymes and receptors. Published studies show that suramin exhibits activity blocking downstream G protein-mediated signaling of various G protein-coupled receptor proteins, including A1 adenosine receptor, D2 receptor, P2 receptor, rhodopsin, and ryanodine receptors (73–76). Suramin was also reported to inhibit human sirtuins (SIRT1/T) (77). Additionally, at high concentrations, suramin has cell-independent effects on blood coagulation and clot formation (64). Whether these mechanisms are involved in endothelial cell protection and improved survival in mice and/or improved acute lung injury caused by histones was not studied here. Because our study was focused on histone-induced microvascular damage and the protective effect of suramin in this context, we did not include mice receiving suramin alone in all experiments. Although this is a limitation to our work, the literature already contains several studies examining the effects of suramin alone. For example, an experimental group receiving suramin alone at a similar dose (60 mg/kg) was included in a previous study that examined effects of suramin on the lung in the context of bleomycin-induced lung injury (78). The mice receiving suramin had no difference in survival from those receiving saline. Furthermore, suramin alone had no impact on total and differential cell count in BALF. This contrasts with the effects of toxic doses of suramin (250–500 mg/kg), which produces abnormal enlargement of lungs and evidence of lung pathology such as the lysosomal storage disorder mucopolysaccharidosis (79, 80). Of note, the combination of histone and suramin produced an ICAM-1 response that appears even lower than with histones alone (Supplemental Fig. 3D). This suggested that the protective effects of suramin in the context of histone exposure may be explained not only by binding histones in solution, but also through other mechanisms of action. In support of this, prior work has shown that suramin alone can decrease immunogenicity of renal endothelial cells by reduction in their expression of ICAM-1

(81). In another study, suramin suppressed cell membrane permeability in cultured kidney cells via inhibitory actions on connexin 43 hemichannels (82). Thus, other known mechanisms of action that are independent of histone exposure, including decreases in ICAM-1 expression and suppression of membrane permeability, may also contribute to the salutary benefits of suramin that we observed.

In summary, we demonstrate a new and previously unreported (to our knowledge) mechanism of action for suramin. Suramin blocks cytotoxic effects of histones and prevents histone-induced vasodilatory dysfunction, endothelial cell activation, thrombin generation, lung injury, and mortality in mice. Our results provide a mechanistic basis and rationale for clinical trials of suramin as a repurposed treatment that can be rapidly deployed to prevent endothelial injury and excessive blood clotting in conditions associated with high circulating histone levels such as trauma and sepsis.

Acknowledgments

We thank Dr. Roxana Del Rio Guerra and the University of Vermont Lamer College of Medicine Flow Cytometry and Cell Sorting Facility.

Disclosures

The authors have no financial conflicts of interest.

References

- Gu, S. X., T. Tyagi, K. Jain, V. W. Gu, S. H. Lee, J. M. Hwa, J. M. Kwan, D. S. Krause, A. I. Lee, S. Halene, et al. 2021. Thrombocytopenia and endotheliopathy: crucial contributors to COVID-19 thromboinflammation. *Nat. Rev. Cardiol.* 18: 194–209.
- Barrett, T. J., M. Cornwell, K. Myndzar, C. C. Rolling, Y. Xia, K. Drenkova, A. Biebuyck, A. T. Fields, M. Tawil, E. Luttrell-Williams, et al. 2021. Platelets amplify endotheliopathy in COVID-19. *Sci. Adv.* 7: eab2434.
- Xu, J., X. Zhang, R. Pelayo, M. Monestier, C. T. Ammollo, F. Semeraro, F. B. Taylor, N. L. Esmon, F. Lupu, and C. T. Esmon. 2009. Extracellular histones are major mediators of death in sepsis. *Nat. Med.* 15: 1318–1321.
- Schumski, A., A. Ortega-Gómez, K. Wichapong, C. Winter, P. Lemnitzer, J. R. Viola, M. Pinilla-Vera, E. Folco, V. Solis-Mezarino, M. Völker-Albert, et al. 2021. Endotoxemia accelerates atherosclerosis through electrostatic charge-mediated monocyte adhesion. *Circulation* 143: 254–266.
- Wu, D., A. Ingram, J. H. Lahti, B. Mazza, J. Grenet, A. Kapoor, L. Liu, V. J. Kidd, and D. Tang. 2002. Apoptotic release of histones from nucleosomes. *J. Biol. Chem.* 277: 12001–12008.
- Allam, R., C. R. Scherbaum, M. N. Darisipudi, S. R. Mulay, H. Hägele, J. Lichtneker, J. H. Hagemann, K. V. Rupanagudi, M. Ryu, C. Schwarzenberger, et al. 2012. Histones from dying renal cells aggravate kidney injury via TLR2 and TLR4. *J. Am. Soc. Nephrol.* 23: 1375–1388.
- Wickman, G. R., L. Julian, K. Mardilovich, S. Schumacher, J. Munro, N. Rath, S. A. Zander, A. Mleczak, D. Sumpton, N. Morrice, et al. 2013. Blebs produced by actin-myosin contraction during apoptosis release damage-associated molecular pattern proteins before secondary necrosis occurs. *Cell Death Differ.* 20: 1293–1305.
- Tsourouktsoglou, T.-D., A. Warnatsch, M. Ioannou, D. Hoving, Q. Wang, and V. Papayannopoulos. 2020. Histones, DNA, and citrullination promote neutrophil extracellular trap inflammation by regulating the localization and activation of TLR4. *Cell Rep.* 31: 107602.
- Zuo, Y., S. Yalavarthi, S. A. Navaz, C. K. Hoy, A. Harbaugh, K. Gockman, M. Zuo, J. A. Madison, H. Shi, Y. Kanthi, and J. S. Knight. 2021. Autoantibodies stabilize neutrophil extracellular traps in COVID-19. *JCI Insight* 6: 150111.
- Knight, J. S., W. Luo, A. A. O'Dell, S. Yalavarthi, W. Zhao, V. Subramanian, C. Guo, R. C. Grenn, P. R. Thompson, D. T. Eitzman, and M. J. Kaplan. 2014. Peptidylarginine deiminase inhibition reduces vascular damage and modulates innate immune responses in murine models of atherosclerosis. *Circ. Res.* 114: 947–956.
- Silvestre-Roig, C., Q. Braster, K. Wichapong, E. Y. Lee, J. M. Teulon, N. Berrebeh, J. Winter, J. M. Adrover, G. S. Santos, A. Froese, et al. 2019. Externalized histone H4 orchestrates chronic inflammation by inducing lytic cell death. *Nature* 569: 236–240.
- Savchenko, A. S., J. I. Borissoff, K. Martinod, S. F. De Meyer, M. Gallant, L. Erpenbeck, A. Brill, Y. Wang, and D. D. Wagner. 2014. VWF-mediated leukocyte recruitment with chromatin decondensation by PAD4 increases myocardial ischemia/reperfusion injury in mice. *Blood* 123: 141–148.
- Brill, A., T. A. Fuchs, A. S. Savchenko, G. M. Thomas, K. Martinod, S. F. De Meyer, A. A. Bhandari, and D. D. Wagner. 2012. Neutrophil extracellular traps promote deep vein thrombosis in mice. *J. Thromb. Haemost.* 10: 136–144.
- Savchenko, A. S., K. Martinod, M. A. Seidman, S. L. Wong, J. I. Borissoff, G. Piazza, P. Libby, S. Z. Goldhaber, R. N. Mitchell, and D. D. Wagner. 2014. Neutrophil extracellular traps form predominantly during the organizing stage of human venous thromboembolism development. *J. Thromb. Haemost.* 12: 860–870.
- Marsman, G., S. Zeerleder, and B. M. Luken. 2016. Extracellular histones, cell-free DNA, or nucleosomes: differences in immunostimulation. *Cell Death Dis.* 7: e2518.
- Silk, E., H. Zhao, H. Weng, and D. Ma. 2017. The role of extracellular histone in organ injury. *Cell Death Dis.* 8: e2812.
- Nakazawa, D., S. V. Kumar, J. Marschner, J. Desai, A. Holderied, L. Rath, F. Kraft, Y. Lei, Y. Fukasawa, G. W. Moeckel, et al. 2017. Histones and neutrophil extracellular traps enhance tubular necrosis and remote organ injury in ischemic AKI. *J. Am. Soc. Nephrol.* 28: 1753–1768.
- Shaw, R. J., S. T. Abrams, J. Austin, J. M. Taylor, S. Lane, T. Dutt, C. Downey, M. Du, L. Turtle, J. K. Baillie, et al. 2021. Circulating histones play a central role in COVID-19-associated coagulopathy and mortality. *Haematologica* 106: 2493–2498.
- Abrams, S. T., N. Zhang, J. Manson, T. Liu, C. Dart, F. Baluwa, S. S. Wang, K. Brohi, A. Kipar, W. Yu, et al. 2013. Circulating histones are mediators of trauma-associated lung injury. *Am. J. Respir. Crit. Care Med.* 187: 160–169.
- Collier, D. M., N. Villalba, A. Sackheim, A. D. Bonev, Z. D. Miller, J. S. Moore, B. Shui, J. C. Lee, F. K. Lee, S. Reining, et al. 2019. Extracellular histones induce calcium signals in the endothelium of resistance-sized mesenteric arteries and cause loss of endothelium-dependent dilation. *Am. J. Physiol. Heart Circ. Physiol.* 316: H1309–H1322.
- Yeung, K. W., P. M. Lau, H. L. Tsang, H. P. Ho, Y. W. Kwan, and S. K. Kong. 2019. Extracellular histones induced eryptotic death in human erythrocytes. *Cell. Physiol. Biochem.* 53: 229–241.
- Meara, C. H. O., L. A. Coupland, F. Kordbacheh, B. J. C. Quah, C. W. Chang, D. A. Simon Davis, A. Bezos, A. M. Browne, C. Freeman, D. J. Hammill, et al. 2020. Neutralizing the pathological effects of extracellular histones with small polyanions. *Nat. Commun.* 11: 6408.
- Villalba, N., S. Baby, B. J. Cha, and S. Y. Yuan. 2020. Site-specific opening of the blood-brain barrier by extracellular histones. *J. Neuroinflammation* 17: 281.
- Allam, R., M. N. Darisipudi, J. Tschopp, and H.-J. Anders. 2013. Histones trigger sterile inflammation by activating the NLRP3 inflammasome. *Eur. J. Immunol.* 43: 3336–3342.
- Semeraro, F., C. T. Ammollo, J. H. Morrissey, G. L. Dale, P. Friese, N. L. Esmon, and C. T. Esmon. 2011. Extracellular histones promote thrombin generation through platelet-dependent mechanisms: involvement of platelet TLR2 and TLR4. *Blood* 118: 1952–1961.
- Shi, C.-X., Y. Wang, Q. Chen, F.-Z. Jiao, M.-H. Pei, and Z.-J. Gong. 2020. Extracellular histone H3 induces pyroptosis during sepsis and may act through NOD2 and VSIG4/NLRP3 pathways. *Front. Cell. Infect. Microbiol.* 10: 196.
- Yang, X., L. Li, J. Liu, B. Lv, and F. Chen. 2016. Extracellular histones induce tissue factor expression in vascular endothelial cells via TLR and activation of NF- κ B and AP-1. *Thromb. Res.* 137: 211–218.
- Meegan, J. E., X. Yang, R. S. Beard, Jr., M. Jannaway, V. Chatterjee, T. E. Taylor-Clark, and S. Y. Yuan. 2018. Citrullinated histone 3 causes endothelial barrier dysfunction. *Biochem. Biophys. Res. Commun.* 503: 1498–1502.
- Pereira, L. F., F. M. Marco, R. Boimorto, A. Caturla, A. Bustos, E. G. De la Concha, and J. L. Subiza. 1994. Histones interact with anionic phospholipids with high avidity; its relevance for the binding of histone-antihistone immune complexes. *Clin. Exp. Immunol.* 97: 175–180.
- Sakharov, D. V., A. F. Jie, M. E. Bekkers, J. J. Emeis, and D. C. Rijken. 2001. Polylysine as a vehicle for extracellular matrix-targeted local drug delivery, providing high accumulation and long-term retention within the vascular wall. *Arterioscler. Thromb. Vasc. Biol.* 21: 943–948.
- Vulliamy, P., S. Gillespie, P. C. Armstrong, H. E. Allan, T. D. Warner, and K. Brohi. 2019. Histone H4 induces platelet ballooning and microparticle release during trauma hemorrhage. *Proc. Natl. Acad. Sci. USA* 116: 17444–17449.
- Henriksen, H. H., S. McGarrity, R. S. Sigurdardóttir, T. Nemkov, A. D'Alessandro, B. O. Palsson, J. Stensballe, C. E. Wade, Ó. Rólfsson, and P. I. Johansson. 2020. Metabolic systems analysis of shock-induced endotheliopathy (SHINE) in trauma: a new research paradigm. *Ann. Surg.* 272: 1140–1148.
- Johansson, P. I., H. H. Henriksen, J. Stensballe, M. Gybel-Brask, J. C. Cardenas, L. A. Baer, B. A. Cotton, J. B. Holcomb, C. E. Wade, and S. R. Ostrowski. 2017. Traumatic endotheliopathy: a prospective observational study of 424 severely injured patients. *Ann. Surg.* 265: 597–603.
- Johansson, P. I., N. A. Windeløv, L. S. Rasmussen, A. M. Sørensen, and S. R. Ostrowski. 2013. Blood levels of histone-complexed DNA fragments are associated with coagulopathy, inflammation and endothelial damage early after trauma. *J. Emerg. Trauma Shock* 6: 171–175.
- Kutcher, M. E., J. Xu, R. F. Vilardi, C. Ho, C. T. Esmon, and M. J. Cohen. 2012. Extracellular histone release in response to traumatic injury: implications for a compensatory role of activated protein C. *J. Trauma Acute Care Surg.* 73: 1389–1394.
- Naumann, D. N., J. Hazeldine, D. J. Davies, J. Bishop, M. J. Midwinter, A. Belli, P. Harrison, and J. M. Lord. 2018. Endotheliopathy of trauma is an on-scene phenomenon, and is associated with multiple organ dysfunction syndrome: a prospective observational study. *Shock* 49: 420–428.
- Naumann, D. N., J. Hazeldine, R. J. Dinsdale, J. R. Bishop, M. J. Midwinter, P. Harrison, S. D. Hutchings, and J. M. Lord. 2017. Endotheliopathy is associated with higher levels of cell-free DNA following major trauma: a prospective observational study. *PLoS One* 12: e0189870.
- Russell, R. T., S. C. Christiaans, T. R. Nice, M. Banks, V. E. Mortellaro, C. Morgan, A. Duhachek-Stapelman, S. J. Lisco, J. D. Kerby, B. M. Wagener, et al. 2018. Histone-complexed DNA fragments levels are associated with coagulopathy, endothelial cell damage, and increased mortality after severe pediatric trauma. *Shock* 49: 44–52.
- McCullough, L. D., M. Roy-O'Reilly, Y.-J. Lai, A. Patrizz, Y. Xu, J. Lee, A. Holmes, D. C. Kraushaar, A. Chauhan, L. H. Sansing, et al. 2021. Exogenous inter- α inhibitor proteins prevent cell death and improve ischemic stroke outcomes in mice. *J. Clin. Invest.* 131: e144898.
- Yang, R., J. Tenhunen, and T. I. Tonnessen. 2017. HMGB1 and histones play a significant role in inducing systemic inflammation and multiple organ dysfunctions in severe acute pancreatitis. *Int. J. Inflamm.* 2017: 1817564.

41. Lv, X., T. Wen, J. Song, D. Xie, L. Wu, X. Jiang, P. Jiang, and Z. Wen. 2017. Extracellular histones are clinically relevant mediators in the pathogenesis of acute respiratory distress syndrome. *Respir. Res.* 18: 165.
42. Zhang, Y., Z. Wen, L. Guan, P. Jiang, T. Gu, J. Zhao, X. Lv, and T. Wen. 2015. Extracellular histones play an inflammatory role in acid aspiration-induced acute respiratory distress syndrome. *Anesthesiology* 122: 127–139.
43. Pati, S., E. Fennern, J. B. Holcomb, M. Barry, A. Trivedi, A. P. Cap, M. J. Martin, C. Wade, R. Kozar, J. C. Cardenas, et al. 2021. Treating the endotheliopathy of SARS-CoV-2 infection with plasma: lessons learned from optimized trauma resuscitation with blood products. *Transfusion* 61(Suppl. 1): S336–S347.
44. Shi, H., A. A. Gandhi, S. A. Smith, Q. Wang, D. Chiang, S. Yalavarthi, R. A. Ali, C. Liu, G. Sule, P.-S. Tsou, et al. 2021. Endothelium-protective, histone-neutralizing properties of the polyanionic agent defibrotide. *JCI Insight* 6: e149149.
45. Pope, W. J. 1924. Synthetic therapeutic agents. *BMJ* 1: 413–414.
46. Daneva, Z., M. Ottolini, Y. L. Chen, E. Klimentova, M. Kuppusamy, S. A. Shah, R. D. Minshall, C. I. Seye, V. E. Laubach, B. E. Isakson, and S. K. Sonkusare. 2021. Endothelial pannexin 1-TRPV4 channel signaling lowers pulmonary arterial pressure in mice. *eLife* 10: e67777.
47. Sonkusare, S. K., A. D. Bonev, J. Ledoux, W. Liedtke, M. I. Kotlikoff, T. J. Heppner, D. C. Hill-Eubanks, and M. T. Nelson. 2012. Elementary Ca²⁺ signals through endothelial TRPV4 channels regulate vascular function. *Science* 336: 597–601.
48. Liao, C., M. Esai Selvan, J. Zhao, J. L. Slimovitch, S. T. Schneebeli, M. Shelley, J. C. Shelley, and J. Li. 2015. Melittin aggregation in aqueous solutions: insight from molecular dynamics simulations. *J. Phys. Chem. B* 119: 10390–10398.
49. Li, J., K. T. McKay, J. M. Remington, and S. T. Schneebeli. 2021. A computational study of cooperative binding to multiple SARS-CoV-2 proteins. *Sci. Rep.* 11: 16307.
50. Bouchard, B. A., and K. Freeman. 2021. Thrombin formation. In *Trauma Induced Coagulopathy*. H. B. Moore, M. D. Neal, and E. E. Moore, eds. Springer International Publishing, Cham, Switzerland, p. 77–84.
51. Malkin, E. Z., and S. V. Bratman. 2020. Bioactive DNA from extracellular vesicles and particles. *Cell Death Dis.* 11: 584.
52. Kleine, T. J., A. Gladfelter, P. N. Lewis, and S. A. Lewis. 1995. Histone-induced damage of a mammalian epithelium: the conductive effect. *Am. J. Physiol.* 268: C1114–C1125.
53. Gamberucci, A., R. Fulceri, P. Marcolongo, W. F. Pralong, and A. Benedetti. 1998. Histones and basic polypeptides activate Ca²⁺/cation influx in various cell types. *Biochem. J.* 331: 623–630.
54. Lam, F. W., M. A. Cruz, K. Parikh, and R. E. Rumbaut. 2016. Histones stimulate von Willebrand factor release in vitro and in vivo. *Haematologica* 101: e277–e279.
55. Kim, J. E., H. J. Yoo, J. Y. Gu, and H. K. Kim. 2016. Histones induce the procoagulant phenotype of endothelial cells through tissue factor up-regulation and thrombomodulin down-regulation. *PLoS One* 11: e0156763.
56. Ammollo, C. T., F. Semeraro, J. Xu, N. L. Esmon, and C. T. Esmon. 2011. Extracellular histones increase plasma thrombin generation by impairing thrombomodulin-dependent protein C activation. *J. Thromb. Haemost.* 9: 1795–1803.
57. Yang, H., A. Kim, T. David, D. Palmer, T. Jin, J. Tien, F. Huang, T. Cheng, S. R. Coughlin, Y. N. Jan, and L. Y. Jan. 2012. TMEM16F forms a Ca²⁺-activated cation channel required for lipid scrambling in platelets during blood coagulation. *Cell* 151: 111–122.
58. Gao, C., R. Xie, C. Yu, R. Ma, W. Dong, H. Meng, Y. Zhang, Y. Si, Z. Zhang, V. Novakovic, et al. 2015. Thrombotic role of blood and endothelial cells in uremia through phosphatidylserine exposure and microparticle release. *PLoS One* 10: e0142835.
59. Wildhagen, K. C. A. A., P. García de Frutos, C. P. Reutelingsperger, R. Schrijver, C. Aresté, A. Ortega-Gómez, N. M. Deckers, H. C. Hemker, O. Soehnlein, and G. A. F. Nicolaes. 2014. Nonanticoagulant heparin prevents histone-mediated cytotoxicity in vitro and improves survival in sepsis. *Blood* 123: 1098–1101.
60. Iba, T., N. Hashiguchi, I. Nagaoka, Y. Tabe, K. Kadota, and K. Sato. 2015. Heparins attenuated histone-mediated cytotoxicity in vitro and improved the survival in a rat model of histone-induced organ dysfunction. *Intensive Care Med.* 3: 36.
61. Pal, P. K., T. Starr, and M. M. Gertler. 1983. Neutralization of heparin by histone and its subfractions. *Thromb. Res.* 31: 69–79.
62. Goligher, E. C., C. A. Bradbury, B. J. McVerry, P. R. Lawler, J. S. Berger, M. N. Gong, M. Carrier, H. R. Reynolds, A. Kumar, A. F. Turgeon, et al.; REMAP-CAP Investigators; ACTIV-4a Investigators; ATTACC Investigators. 2021. Therapeutic anticoagulation with heparin in critically ill patients with Covid-19. *N. Engl. J. Med.* 385: 777–789.
63. Lawler, P. R., E. C. Goligher, J. S. Berger, M. D. Neal, B. J. McVerry, J. C. Nicolau, M. N. Gong, M. Carrier, R. S. Rosenson, H. R. Reynolds, et al.; REMAP-CAP Investigators; ACTIV-4a Investigators; ATTACC Investigators. 2021. Therapeutic anticoagulation with heparin in noncritically ill patients with Covid-19. *N. Engl. J. Med.* 385: 790–802.
64. Horne III, M. K., O. J. Wilson, M. Cooper, H. R. Galnick, and C. E. Myers. 1992. The effect of suramin on laboratory tests of coagulation. *Thromb. Haemost.* 67: 434–439.
65. Daigo, K., M. Nakakido, R. Ohashi, R. Fukuda, K. Matsubara, T. Minami, N. Yamaguchi, K. Inoue, S. Jiang, M. Naito, et al. 2014. Protective effect of the long pentraxin PTX3 against histone-mediated endothelial cell cytotoxicity in sepsis. *Sci. Signal.* 7: ra88.
66. Wygrecka, M., D. Kosanovic, L. Wujak, K. Reppe, I. Henneke, H. Frey, M. Didiashvili, G. Kwapiszewska, L. M. Marsh, N. Baal, et al. 2017. Antihistone properties of C1 esterase inhibitor protect against lung injury. [Published erratum appears in 2022 *Am. J. Respir. Crit. Care Med.* 206: 1184.] *Am. J. Respir. Crit. Care Med.* 196: 186–199.
67. Lam, F. W., M. A. Cruz, H.-C. E. Leung, K. S. Parikh, C. W. Smith, and R. E. Rumbaut. 2013. Histone induced platelet aggregation is inhibited by normal albumin. *Thromb. Res.* 132: 69–76.
68. Bouchard, B. A., C. Colovos, M. Lawson, Z. Osborn, A. Sackheim, K. J. Mould, W. J. Janssen, M. J. Cohen, D. Majumdar, and K. Freeman. 2021. Increased histone-DNA complexes and endothelial-dependent thrombin generation in severe COVID-19. *Vascul. Pharmacol.* 142: 106950.
69. Fatmi, S., L. Taouzin, M. Skiba, and M. Iguer-Ouada. 2021. The use of cyclodextrin or its complexes as a potential treatment against the 2019 novel coronavirus: a mini-review. *Curr. Drug Deliv.* 18: 382–386.
70. Jaimes, F., G. De La Rosa, C. Morales, F. Fortich, C. Arango, D. Aguirre, and A. Muñoz. 2009. Unfractionated heparin for treatment of sepsis: a randomized clinical trial (The HETRASE Study). *Crit. Care Med.* 37: 1185–1196.
71. Sayburn, A. 2020. Covid-19: trials of four potential treatments to generate “robust data” of what works. *BMJ* 368: m1206.
72. Zhu, W., M. Xu, C. Z. Chen, H. Guo, M. Shen, X. Hu, P. Shinn, C. Klumpp-Thomas, S. G. Michael, and W. Zheng. 2020. Identification of SARS-CoV-2 3CL protease inhibitors by a quantitative high-throughput screening. *ACS Pharmacol. Transl. Sci.* 3: 1008–1016.
73. Waldhoer, M., E. Bofill-Cardona, G. Milligan, M. Freissmuth, and C. Nanoff. 1998. Differential uncoupling of A1 adenosine and D2 dopamine receptors by suramin and didemethylated suramin (NF037). *Mol. Pharmacol.* 53: 808–818.
74. Lehmann, N., G. Krishna Aradhya, and K. Fahmy. 2002. Suramin affects coupling of rhodopsin to transducin. *Biophys. J.* 82: 793–802.
75. Hohenegger, M., M. Matyash, K. Poussu, A. Herrmann-Frank, S. Sarközi, F. Lehmann-Horn, and M. Freissmuth. 1996. Activation of the skeletal muscle ryanodine receptor by suramin and suramin analogs. *Mol. Pharmacol.* 50: 1443–1453.
76. Leff, P., B. E. Wood, and S. E. O'Connor. 1990. Suramin is a slowly-equilibrating but competitive antagonist at P2x-receptors in the rabbit isolated ear artery. *Br. J. Pharmacol.* 101: 645–649.
77. Manjula, R., K. Anuja, and F. J. Alcaín. 2021. SIRT1 and SIRT2 activity control in neurodegenerative diseases. *Front. Pharmacol.* 11: 585821.
78. Lossos, I. S., G. Izbicki, R. Or, R. H. Goldstein, and R. Breuer. 2000. The effect of suramin on bleomycin-induced lung injury. *Life Sci.* 67: 2873–2881.
79. Rees, S., G. Constantopoulos, J. A. Barranger, and R. O. Brady. 1982. Organomegaly and histopathology in an animal model of mucopolysaccharidosis induced by suramin. *Naunyn-Schmiedeberg's Arch. Pharmacol.* 319: 262–270.
80. Rees, S., G. Constantopoulos, and R. O. Brady. 1986. The suramin-treated rat as a model of mucopolysaccharidosis. Variation in the reversibility of biochemical and morphological changes among different organs. *Virchows Arch. B Cell Pathol. Incl. Mol. Pathol.* 52: 259–272.
81. Trieb, K., K. Dorfinger, N. Neuhold, E. Selzer, A. Wilfing, S. Czernin, M. Hermann, B. Niederle, A. Gessl, H. Vierhapper, et al. 1992. Suramin affects differentiated and undifferentiated human thyroid epithelial cells in vitro. *J. Endocrinol.* 134: 505–511, NP.
82. Chi, Y., K. Gao, H. Zhang, M. Takeda, and J. Yao. 2014. Suppression of cell membrane permeability by suramin: involvement of its inhibitory actions on connexin 43 hemichannels. *Br. J. Pharmacol.* 171: 3448–3462.